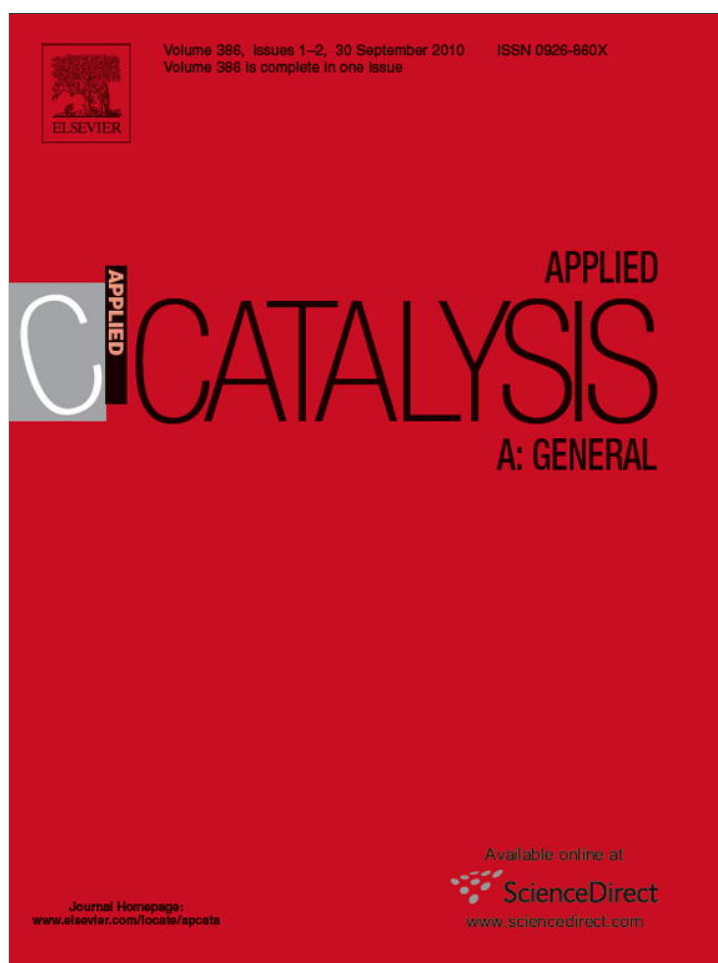


Provided for non-commercial research and education use.  
Not for reproduction, distribution or commercial use.



This article appeared in a journal published by Elsevier. The attached copy is furnished to the author for internal non-commercial research and education use, including for instruction at the authors institution and sharing with colleagues.

Other uses, including reproduction and distribution, or selling or licensing copies, or posting to personal, institutional or third party websites are prohibited.

In most cases authors are permitted to post their version of the article (e.g. in Word or Tex form) to their personal website or institutional repository. Authors requiring further information regarding Elsevier's archiving and manuscript policies are encouraged to visit:

<http://www.elsevier.com/copyright>



## Ethylbenzene production over platinum catalysts supported on modified KY zeolites

Juliana da Silva Lima Fonseca<sup>a</sup>, Arnaldo da Costa Faro Júnior<sup>b</sup>,  
Javier Mario Grau<sup>c</sup>, Maria do Carmo Rangel<sup>a,\*</sup>

<sup>a</sup> GECCAT - Grupo de Estudo em Cinética e Catálise, Instituto de Química, Universidade Federal da Bahia, Campus Universitário de Ondina, Federação, 40 170-290, Salvador, Bahia, Brazil

<sup>b</sup> Departamento de Físico-Química, Instituto de Química, Universidade Federal do Rio de Janeiro, Ilha do Fundão, CT, Bloco A, 21 949-900, Rio de Janeiro, RJ, Brazil

<sup>c</sup> Instituto de Investigaciones en Catálisis y Petroquímica - INCAPE (FIQ, UNL-CONICET), Santiago del Estero 2654, S3000AOJ, Santa Fe, Argentina

### ARTICLE INFO

#### Article history:

Received 25 March 2010

Received in revised form 27 July 2010

Accepted 29 July 2010

Available online 6 August 2010

#### Keywords:

*n*-Octane reforming

Y zeolite

Ethylbenzene

Coke

Barium

Calcium

Magnesium

### ABSTRACT

Platinum catalysts supported on zeolite KY (Si/Al = 12.7), modified with magnesium, calcium or barium, were evaluated in *n*-octane reforming to produce ethylbenzene. The catalysts were characterized by nitrogen adsorption, <sup>27</sup>Al and <sup>29</sup>Si solid state nuclear magnetic resonance, Fourier transform infrared spectroscopy using carbon monoxide or pyridine, metal dispersion measurements and programmed temperature oxidation. No significant structural change was noted for the solids due to the dopants except for barium, which decreased the specific surface area, due to the partial blockage of the zeolite channels by the large size ions. However, a decrease was noted for all samples due to platinum, which partially blocked the zeolite channels. Barium also decreased the crystallinity while platinum caused this effect only for calcium and barium-containing samples, due to the structure partial collapse. Metallic platinum species in several electronic states were detected in the cages of zeolite, barium-containing catalyst showing the most electron-enriched platinum atoms. The amount of Lewis and Brønsted acid sites increased due to magnesium and calcium but barium increased only the amount of Lewis acid sites, as compared to potassium-containing solid. The catalysts with magnesium and barium showed the same platinum dispersion, which was higher than the one containing calcium. All catalysts were active in *n*-octane reforming at 723 K and selective to ethylbenzene, but the conversion dropped with time reaction due to the decrease of specific surface area and to coke deposition. The calcium-containing sample produced the hardest coke, which led to the highest drop in conversion. The *n*-octane conversion was supposed to occur by a monofunctional mechanism but the bifunctional mechanism also seemed to occur due to the residual acidity of the catalysts. The calcium and barium-containing catalysts were the most selective to ethylbenzene, due to electron-enriched platinum species related to promoters, but the low ethylbenzene selectivity for the magnesium-containing catalyst was compensated by its high conversion, resulting in similar yields for all catalysts.

© 2010 Elsevier B.V. All rights reserved.

### 1. Introduction

Ethylbenzene production is one of the most important large volume processes in the modern petrochemical industry, with around 23 million metric tons per year [1]. Most of this production goes to the dehydrogenation process in the presence of steam to get styrene, which further goes through polymerization to generate polystyrene and other high value polymers for several applications [2–4].

The current technology of ethylbenzene production, proposed by Lummus/Unocal/UOP, adopts a liquid-phase alkylation process

in which ethylbenzene is obtained by benzene alkylation with ethene over a zeolite catalyst. This process is performed at low temperatures and high pressures and the liquid-phase operation has the advantage of a better control and a longer catalyst life [1,2,5,6]. In addition, it avoids the drawbacks of the traditional process whose catalysts were strong mineral acids or Lewis acids, which are toxic and corrosive, making dangerous their handling and transport [6]. When the first commercial plant was started-up, in 1990, a Y-type zeolite was used but the last generation of these catalysts is based on modified beta-type zeolite, which allowed to overcome the diffusion constraints, being more selective than Y zeolite [6,7].

In spite of these advantages, this process uses high value chemicals, such as ethene and benzene, which increases the costs for manufacturing ethylbenzene. A more attractive option could be the production of ethylbenzene from a starting material com-

\* Corresponding author.

E-mail address: [mcarmov@ufba.br](mailto:mcarmov@ufba.br) (M.d.C. Rangel).

ing directly from the distillation of petroleum, for instance, by the dehydrocyclization of petroleum naphtha cuts, rich in linear paraffins with eight carbon atoms. This route seems to be more economic, since it does not need high value chemicals.

Under the conditions of conventional naphtha reforming in petroleum refineries, aromatics are produced in the process through *n*-octane dehydrocyclization reaction [8–13]. In addition, it has been recognized for more than 25 years that the aromatization of *n*-alkanes is an important route to obtain high value aromatics [14]. Several studies have shown that the catalysts must fit some requirements in order to maximize ethylbenzene production, such as low surface acidity to avoid cracking and isomerization [15], ability of the support to stabilize the well dispersed metal as very small particles [15,16] and a pore system unable to favor the formation of large amounts of coke, which could lead to catalyst deactivation [17,18]. Various catalysts seem to show these features and have been proven to be efficient for producing ethylbenzene, such as zirconia and carbon [19], nanoparticles of titania, zirconia and hafnium oxide embedded in a carbon matrix [20], potassium-doped alumina-supported platinum [21], zirconia and alumina-supported platinum and platinum-tin [22], silica or silicalite-supported platinum [23], platinum supported on non-acidic spinel oxides like  $\text{MgAl}_2\text{O}_4$  or  $\text{ZnAl}_2\text{O}_4$  [24],  $\text{Mo}_2\text{C}$ -containing catalysts [25] and platinum supported on several kinds of zeolites [14].

Among these solids, zeolites seem to be specially promising to the reaction due to the possibility of the easy control of their acidity and the morphology and size of the channels, as well as of the size and distribution of the metal particles that can be deposited inside or outside the channels. In fact, several authors [14,16] have recognized the importance of these features in affecting the performance of these catalysts in the aromatization of *n*-octane. Jongpatiwut et al. [14], for instance, compared the performance of several non-acidic large pore zeolite in the *n*-octane aromatization and recognized the potential of Pt-K/LTL and Pt-K-FAU which exhibited the highest activity and aromatics selectivity.

In order to get more efficient catalysts for the production of ethylbenzene from *n*-octane dehydrocyclization, the effect of magnesium, calcium and barium on the properties of Y zeolite-supported platinum was studied in this work. It is well known that the addition of promoters is an efficient way to change the acidity of zeolites [26,27].

## 2. Experimental

### 2.1. Catalysts preparation

A commercial HY zeolite (Zeolist) with a high Si/Al ratio (12.7) was used as the support. This solid was submitted to ion exchange with potassium by its dispersion (100 g) in 700 mL of a potassium chloride aqueous solution ( $0.027 \text{ g L}^{-1}$ ) at room temperature and keeping it under stirring for 4 h. Then, the suspension was filtered and the precipitate was washed with deionized water up to the complete removal of chloride ions, confirmed through tests with a silver nitrate solution ( $1 \text{ mol L}^{-1}$ ). The solid was dried for 4 h at 393 K and calcined at 473 K for 12 h, under air flow ( $300 \text{ mL min}^{-1}$ ) to get a support named KY. The Mg/KY, Ca/KY and Ba/KY samples were obtained by impregnating the KY sample with magnesium nitrate ( $\text{Mg}(\text{NO}_3)_2 \cdot 6\text{H}_2\text{O}$ ), calcium nitrate ( $\text{Ca}(\text{NO}_3)_2 \cdot 4\text{H}_2\text{O}$ ) and barium nitrate ( $\text{Ba}(\text{NO}_3)_2$ ), respectively, using incipient wetness impregnation at room temperature. The volume and concentration of the solutions (1.3 mL of solution/g of zeolite) were calculated so that the final concentration (weight percentage) of each metal was 0.50% of magnesium, 0.82% of calcium and 2.82% of barium, corresponding to a promoter to platinum ratio of 4. After the impregnation, the solids were kept at room temperature for 12 h

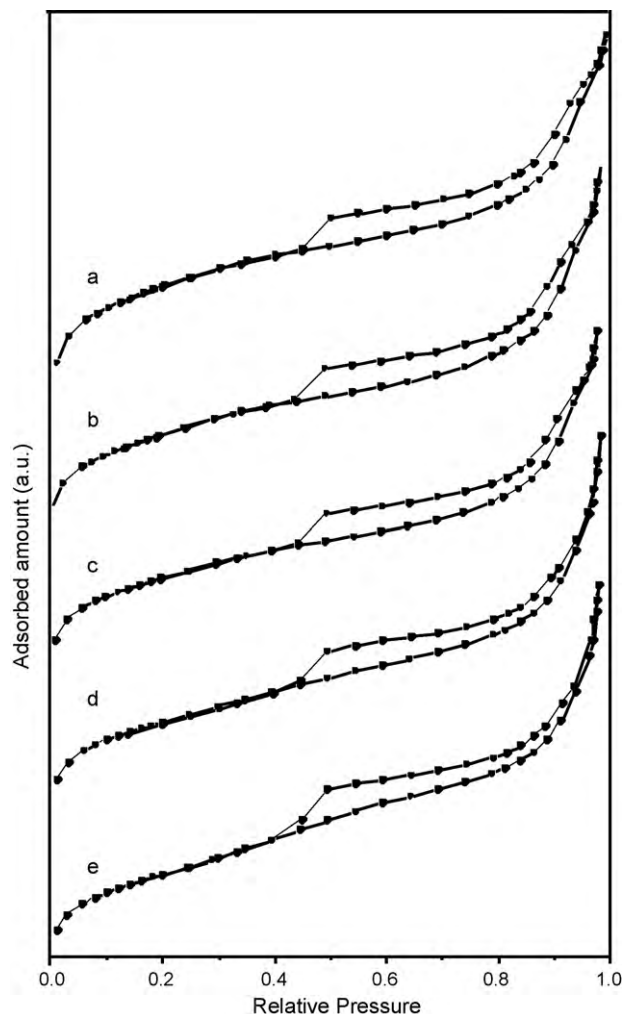


Fig. 1. Adsorption isotherms of nitrogen for the samples: (a) KY; (b) Pt/KY; (c) PtMg/KY; (d) PtCa/KY and (e) PtBa/KY.

and dried at 383 K for more 12 h. The samples was heated under air flow ( $20 \text{ cm}^3 \text{ min}^{-1}$ ) up to 453 K ( $2 \text{ K min}^{-1}$ ), kept at this temperature for 2 h, then heated ( $2 \text{ K min}^{-1}$ ) up to 673 K, kept at this temperature for 2 h and finally heated ( $5 \text{ K min}^{-1}$ ) up to 873 K being kept at this temperature for 4 h.

Platinum was added to the solids by the incipient wetness method using tetramineplatinum II nitrate,  $(\text{Pt}(\text{NH}_3)_4(\text{NO}_3)_2)$ , to obtain samples with 1% (w/w) of platinum. After impregnation, the sample was kept at room temperature for 12 h and then heated at 393 K for 4 h, followed by calcination under air flow ( $100 \text{ cm}^3 \text{ min}^{-1}$ ). Afterwards, it was heated at  $2 \text{ K min}^{-1}$  up to 453 K, remaining at this temperature for 2 h and heated again at  $2 \text{ K min}^{-1}$  up to 623 K, remaining at this temperature for 4 h.

Table 1

Textural properties of parent and modified solids.

Sample	Sg ( $\text{m}^2 \text{ g}^{-1}$ )	Micropore volume ( $\text{cm}^3 \text{ g}^{-1}$ )	Mesopore volume ( $\text{cm}^3 \text{ g}^{-1}$ )
KY	738	0.242	0.196
Pt/KY	708	0.232	0.198
Mg/KY	689	0.231	0.198
Ca/KY	687	0.226	0.192
Ba/KY	616	0.208	0.184
PtMg/KY	629	0.203	0.193
PtCa/KY	610	0.185	0.233
PtBa/KY	482	0.125	0.256

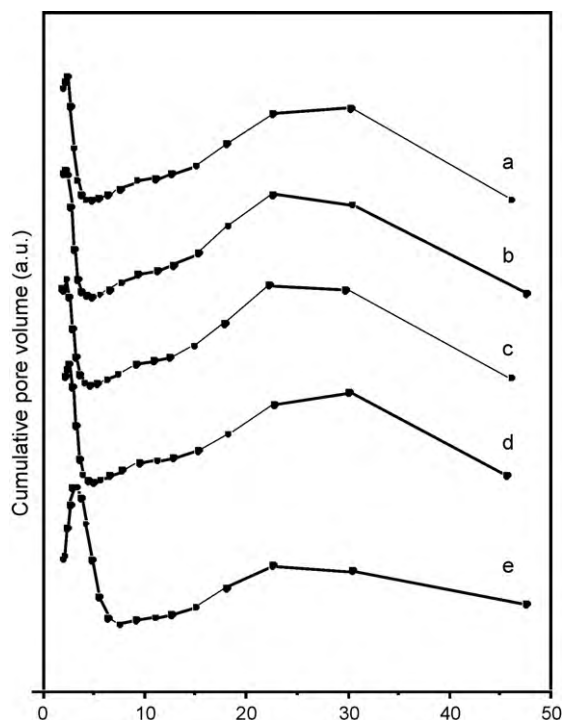


Fig. 2. Mesopore size distributions for the samples: (a) KY; (b) Pt/KY; (c) PtMg/KY; (d) PtCa/KY and (e) PtBa/KY.

The impregnated solid was reduced under hydrogen flow ( $20 \text{ cm}^3 \text{ min}^{-1}$ ) at a heating rate of  $2 \text{ min}^{-1}$  up to  $723 \text{ K}$  and kept at this temperature for  $4 \text{ h}$ . The solids produced were called PtMg/KY, PtCa/KY and PtBa/KY.

In order to obtain samples with the minimum possible amount of acidic sites, the samples went through another ion exchange, by the same procedure described. The new samples obtained were called PtMg/KY(IE), PtCa/KY(IE) and PtBa/KY(IE).

## 2.2. Characterization of the Samples

The specific surface area and porosity measurements were carried out by nitrogen adsorption at  $77 \text{ K}$ , in a Micromeritics equipment, model ASAP 2010. The specific surface areas were calculated using the BET model while the micropores volume was calculated by the  $t$ -plot method, using the Harkins and Jura equation. The BJH method was used to calculate the mesopores volume and the pore size distribution, using the adsorption curve. Before the analysis,  $0.2 \text{ g}$  of the sample was heated up to  $473 \text{ K}$  under vacuum in order to remove water from the zeolite. After the catalytic test, the specific surface areas of the spent catalysts were measured again.

X-ray diffraction measurements were performed at room temperature in a Shimadzu XD3A model equipment, working with a nickel filter and  $\text{CuK}\alpha$  radiation ( $\lambda = 1.54056 \text{ \AA}$ ), generated at  $30 \text{ kV}$  and  $20 \text{ mA}$ . The diffractograms were obtained within the range of  $2\theta = 5\text{--}50^\circ$  diffraction angles, with a scanning velocity of  $2 \text{ K min}^{-1}$ .

The nuclear magnetic resonance spectroscopy analyses were carried out in a Bruker equipment, model DRX-300 ( $7.05 \text{ T}$ ). The spectra were obtained with a CP-MAS Bruker, multinuclear probe, with zirconium rotors of  $4 \text{ mm}$  and  $4$  and  $7 \text{ kHz}$  rotation frequencies were used with  $^{29}\text{Si}$  and  $^{27}\text{Al}$  nuclei, respectively. The measurements of  $^{27}\text{Al}$  were performed with  $3000$  scans and pulses of  $0.3 \text{ s}$ , the measurements for  $^{29}\text{Si}$  were taken using  $1000$  scans and  $10 \text{ s}$  pulses.

The experiments of Fourier transform infrared spectroscopy were performed at room temperature in a PerkinElmer spectropho-

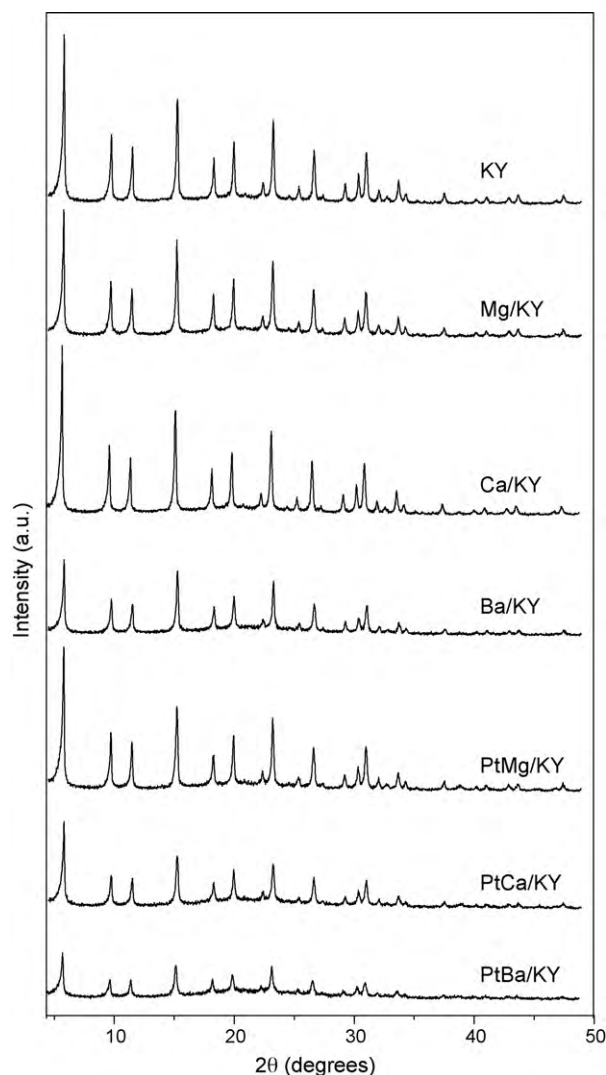


Fig. 3. X-ray diffractograms for the samples: (a) KY; (b) Mg/KY; (c) Ca/KY; (d) Ba/KY; (e) PtMg/KY; (f) PtCa/KY and (g) PtBa/KY.

tometer, model Spectrum One. For spectral acquisition,  $32$  scans were carried out, with a resolution of  $4.0 \text{ cm}^{-1}$ , in the region between  $400$  and  $4000 \text{ cm}^{-1}$ . The samples were diluted in potassium bromide ( $100 \text{ mg KBr/mg}$  of sample), pressed and the wafers obtained were analyzed for studying bands related to structural variations of zeolites and to check the changes in the structure after the different treatments, as well as to calculate the Si/Al ratio, as proposed by Sohn et al. [28]. For studying the hydroxyl stretching region of the spectra, the samples were prepared as self-supported wafers and pre-treated under vacuum ( $10^{-5} \text{ Torr}$ ). Then they were heated from room temperature up to  $623 \text{ K}$  ( $5 \text{ K min}^{-1}$ ) to remove water from the zeolite.

While using carbon monoxide as a probe molecule, samples were prepared as self-supported wafers and reduced under hydrogen flow up to  $623 \text{ K}$ . After reduction, the sample was kept at  $623 \text{ K}$ , for  $1 \text{ h}$ . Then, it was cooled down to room temperature and the first spectrum was recorded. Carbon monoxide was added to the cell (until obtaining a  $15 \text{ Torr}$  increment on pressure) and, after a period of equilibration ( $5 \text{ min}$ ), the sample was evacuated for  $2 \text{ min}$  to remove physisorbed carbon monoxide; then a second spectrum was recorded. The spectrum of carbon monoxide chemisorbed on the catalyst was obtained by subtracting these two spectra.

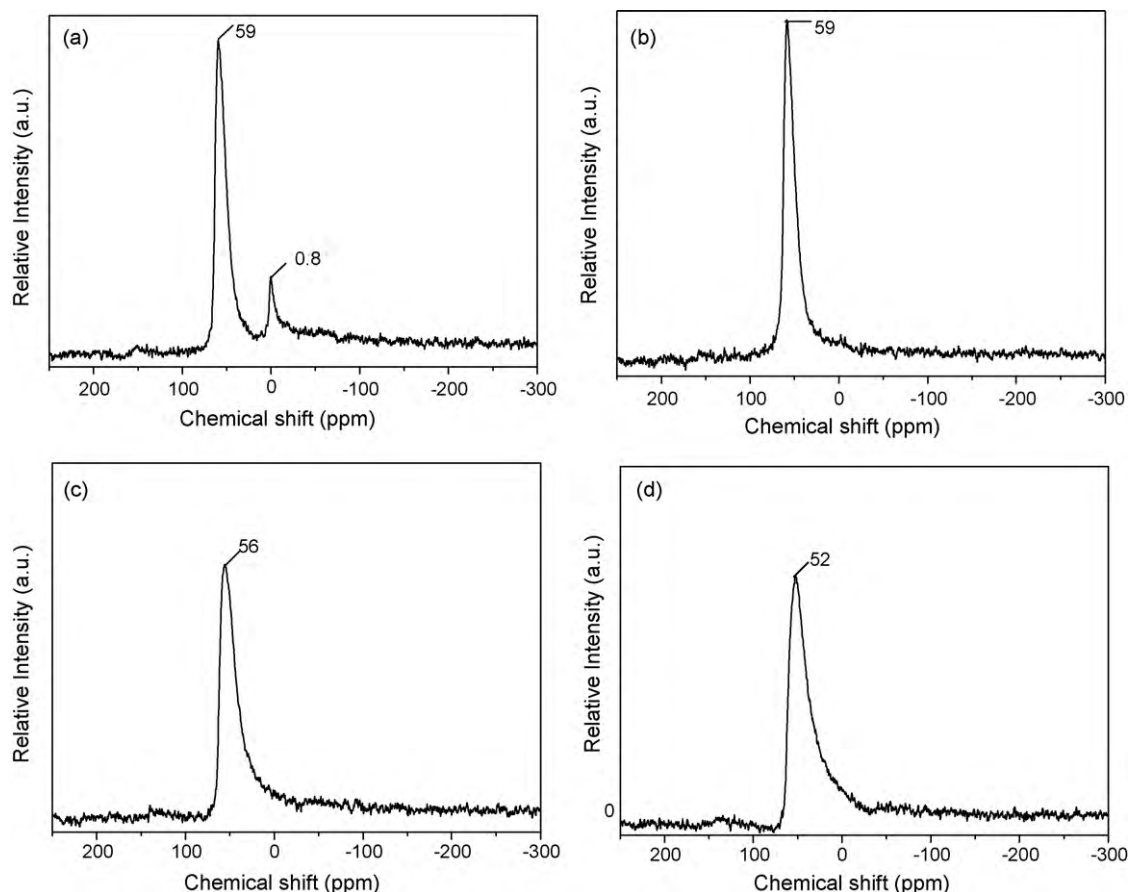


Fig. 4.  $^{27}\text{Al}$ -NMR spectra for the samples: (a) HY; (b) PtMg/KY; (c) PtCa/KY and (d) PtBa/KY.

In the studies performed with adsorbed pyridine, samples were also prepared as self-supported wafers and were pre-treated under a vacuum of  $10^{-5}$  Torr, at 623 K. After cooling down to room temperature, the first spectrum was obtained. Then, the cell was reconnected to the vacuum line and pyridine vapor was admitted (until reaching a 1 Torr pressure increment) and kept in contact with the sample at 323 K, during an equilibration period of 5 min after the beginning of adsorption. Next, the first spectrum was obtained for the sample with adsorbed pyridine. The same wafer was submitted to vacuum again ( $10^{-5}$  Torr), at different temperatures (373, 473, 573 and 673 K) for 10 min at each temperature and a spectrum was obtained at room temperature after each evacuation. The amounts of acid sites were calculated from the integrated molar extinction coefficient (IMEC) taking into account the diameter and mass of each wafer [29].

The metal dispersion of the catalysts was determined from hydrogen chemisorption isotherms, obtained at 308 K. In the experiments, approximately 0.5 g of the sample were added in a quartz reactor for analysis in a Micromeritics equipment, model ASAP 2010. The dispersion of the metal was calculated considering that hydrogen dissociative adsorption occurs on platinum.

After the catalytic tests, temperature-programmed oxidation (TPO) was carried out on samples used in the reaction. The equipment consisted of an oven, a reactor and a methanator, containing Ni/kieselguhr as catalyst. Deposited coke was burned and transformed into carbon dioxide, which was transformed into methane by going through the methanator, together with hydrogen. The signal, due to the methane generated, was then detected by a FID detector and processed in a computer. An experiment with a sample containing a known carbon concentration was performed to calculate the quantity of carbon in each sample.

### 2.3. Catalysts evaluation

The catalyst performance measurements for the *n*-octane reforming were carried out in a micro catalytic unit, comprised of a tubular fixed-bed quartz reactor, operated at 723 K and atmospheric pressure. The *n*-octane reactant was fed to the system by means of a Cole–Palmer dosing pump (Single-Syringe Infusion Pump P-74900-05) and the analysis system was comprised of a Shimadzu gas-chromatograph, with a squalene capillary column.

Before reaction, the catalysts were reduced in situ, under hydrogen flow at 723 K, with a heating rate of  $5\text{ K min}^{-1}$ , for 1 h. After reduction, the temperature was kept at 723 K and the catalytic reaction started under hydrogen flow ( $80\text{ mL min}^{-1}$ ), using a catalyst mass of 0.16 g and an *n*-octane flow rate of  $0.8\text{ mL h}^{-1}$ . The hydrogen to *n*-octane molar ratio was of 7.3 and the space velocity (WHSV) was of  $3.4\text{ h}^{-1}$ .

## 3. Results and discussion

Fig. 1 shows the nitrogen adsorption and desorption isotherms for the samples. These curves are classified as intermediate isotherms, between the types I and IV by the Brunauer classification, which are related to microporous materials containing mesopores. A typical isotherm of the microporous solids was expected for Y zeolite [30] but the hysteresis loop indicates also the presence of mesopores. All the curves were similar, indicating that there were no significant structural changes in these solids with the addition of the dopants and of platinum. As observed in Fig. 2, mesopores distribution curves of the samples were not altered either by the addition of metals to the support. The curves show a peak near

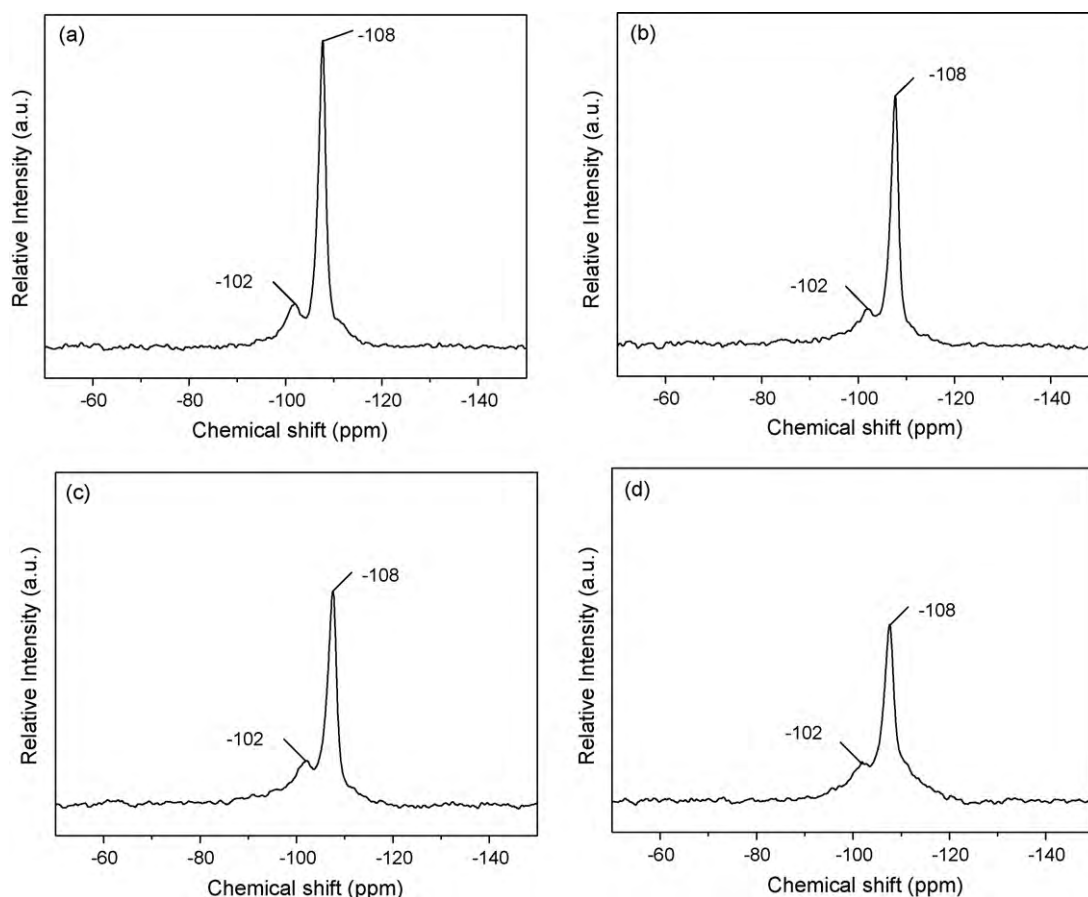


Fig. 5.  $^{29}\text{Si}$ -NMR spectra for the samples: (a) HY; (b) PtMg/KY; (c) PtCa/KY and (d) PtBa/KY.

2 nm and a wide distribution range for mesopores, between 15 and 35 nm.

Table 1 displays the results of specific surface area, as well as of micropores and mesopores volume of samples. The incorporation of magnesium and calcium did not significantly alter the specific surface area of KY zeolite, but the addition of barium caused a decrease. This result is probably a consequence of the bigger size of the barium ion, when compared to the other promoters; it seems that this species is large enough to cause a partial blockage of the zeolite channels, making the accessibility of nitrogen to the pores more difficult. In all cases, there was a decrease of the specific surface areas when platinum was added to samples containing promoters; however, most of the specific surface area is still accessible. This decrease can be ascribed to the platinum agglomerates that may be partially clogging the zeolite channels. The sample with barium showed the highest decrease on this parameter, probably due to the ion size, which, together with platinum, enhanced the blockage of zeolite channels.

The micropores volume (Table 1) was not significantly altered by the addition of platinum or the promoters, except for barium, which led to a 14% decrease, as compared to the KY sample. All catalysts showed variation in micropores volume, in agreement with the results of specific surface area, suggesting that this decrease was caused by micropores blockage. Regarding mesopores volume, no significant variation was observed due to the incorporation of promoters and platinum, except for the samples containing calcium and barium, which showed an increment in the mesopores volume, a probable consequence of a partial collapse of the zeolite structure during platinum addition, calcination or reduction.

The X-ray diffractograms showed typical profiles of Y zeolite, as illustrated in Fig. 3. The incorporation of promoters did not alter

the KY zeolite diffraction profile although a crystallinity loss was observed with the addition of barium. When adding platinum to the solids, a crystallinity loss was observed only for the catalysts containing calcium and barium, because of the structure partial collapse, in accordance with the textural analysis results. No peak related neither to platinum species, nor to promoters was observed.

Fig. 4 shows the  $^{27}\text{Al}$  RMN-MAS spectra of samples. In all cases, an intense peak is observed in the range of 59–52 ppm, ascribed to aluminum atoms in the zeolite framework in tetrahedral sites [26,31]. A peak at 0.8 ppm was also noted in the spectrum of the HY sample, typical of extra-framework aluminum in octahedral coordination [26,31]. The catalysts containing promoters did not show any peak related to aluminum nuclei in a defined octahedral coordination but an extension of the main peak near 0 ppm could be observed, which may indicate the presence of residual extra-framework aluminum species.

The  $^{29}\text{Si}$  RMN-MAS spectrum of HY sample (Fig. 5) displayed two peaks at –102 and –108 ppm. The least intense peak (–102 ppm) is ascribed to the silicon nucleus bonded to three other silicon nuclei and to one aluminum nucleus (Si(1Al)), while the most intense (–108 ppm) is related to the silicon nucleus bonded to other four silicon nuclei and no aluminum (Si(0Al)) [32]. Samples containing platinum also showed spectra with these two peaks. The qualitative analysis of the spectra suggests that these samples are very dealuminated, since the peak related to Si(0Al) is much more intense than the one related to Si(1Al); also, there are no peaks associated with Si(2Al), Si(3Al) or Si(4Al). In addition, values in the range of 18.3 and 21.2 were found when calculating the Si/Al ratio [31], evidencing a high degree of dealumination. These results are not in accordance with the nominal value (12.7) but other authors [33] showed that at high Si/Al ratios the extremely intense Si(0Al) peak renders the

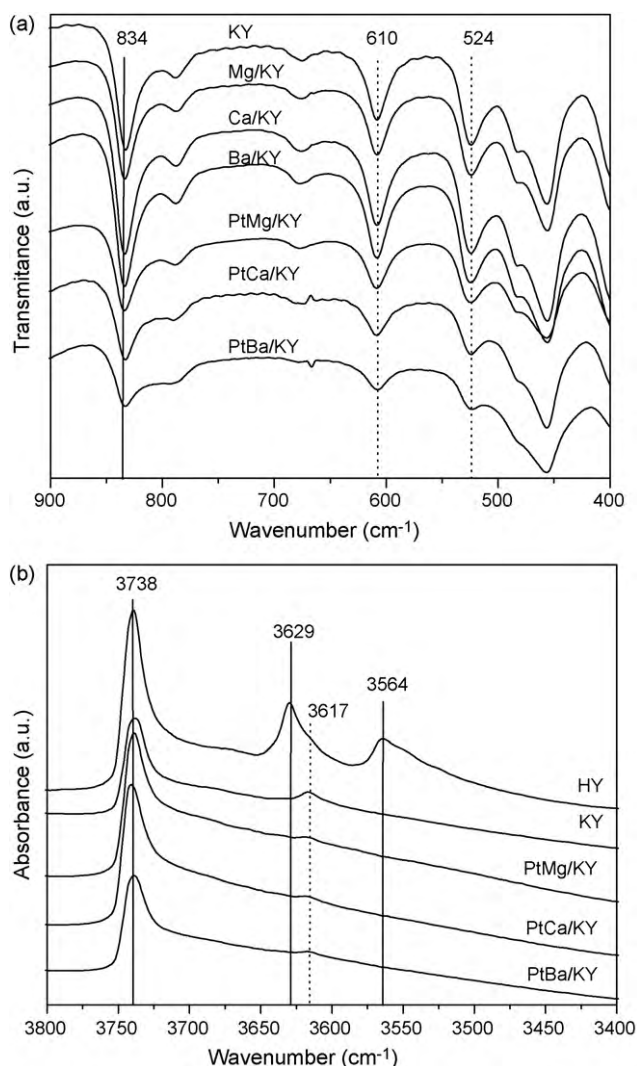


**Fig. 6.** FTIR spectra for the samples: (a) in the region of structural vibrations and (b) in the region of the hydroxyl vibrations.

Si(1Al) peak difficult to be integrated, which may lead to errors in the Si/Al ratio calculation. Meanwhile, there is no evidence of dealumination of the zeolite framework due to the addition of metals. Besides, there is an influence of the silanol groups (Si–OH), which are present in high amounts in this zeolite, occurring with the same frequency of Si(OAl) groups.

The infrared spectra of the samples are shown in Fig. 6(a), for the range of 900–400  $\text{cm}^{-1}$ . The band between 420 and 500  $\text{cm}^{-1}$  is ascribed to the T–O bond vibration (where T may be silicon or aluminum), which is not sensitive to structural variations while that near 610  $\text{cm}^{-1}$  is related to the presence of double rings in zeolite structure, being sensitive to variations in the structure [34]. The band at 524  $\text{cm}^{-1}$  is related to an external bond of the double rings with six members and becomes less intense for PtCa/KY and PtBa/KY samples, a fact which is associated to the partial loss of crystallinity [35].

On the other hand, the stretching near 834  $\text{cm}^{-1}$  is sensitive to Si/Al ratio in the framework and can be shifted to lower frequencies by increasing the amount of aluminum atoms in tetrahedral coordination, due to the decrease of the average force constant of T–O bonds [26,28,36]. As silicon is more electronegative than aluminum, the T–O bond lengths vary from one species to another, the Al–O bond length being 0.174 nm and the Si–O bond 0.160 nm [37]. From Fig. 6, it can be observed that all samples showed this stretch-

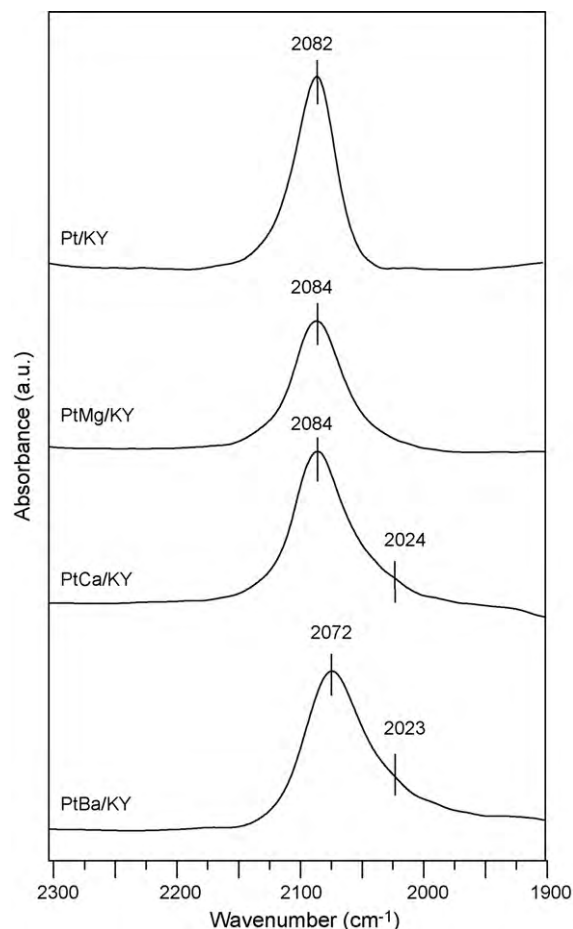


**Fig. 7.** FTIR spectra of adsorbed carbon monoxide on the samples.

ing near 834  $\text{cm}^{-1}$ , suggesting that there was no significant change in the concentration of aluminum atoms in the zeolite framework.

The amount of aluminum atoms can be calculated from the frequencies of O–T–O bonds stretching and, thus, the Si/Al ratio of zeolites [28] can also be deduced. The Si/Al ratio obtained varies between 11.3 and 12.0, very close to the nominal value (12.7). It can thus be concluded that there was no significant change for the Si/Al ratio in samples, as compared to the precursor solid (KY).

The infrared spectra in the hydroxyl stretching region are shown in Fig. 6(b). A band at 3738  $\text{cm}^{-1}$  was observed for the HY sample, ascribed to the inner silanol groups. High frequency bands at 3629  $\text{cm}^{-1}$  were also observed, related to the vibration of hydroxyl groups in the (Si(OH)Al) bond within the zeolite supercages. A band at 3567  $\text{cm}^{-1}$  was noted at lower frequency, due to the vibration of these groups in the small cavities [29,33,36,38]. There is a controversy about the exact position of the hydroxyl groups related to the vibration bands at low frequencies. Breck [36] stated that these groups are located in sodalite cages, while Thibault-Starzyk et al. [38] proposed that they are in the hexagonal prisms of the Y zeolite. As KY, PtMg/KY, PtCa/KY and PtBa/KY samples were submitted to ion exchange, they were not expected to show hydroxyl groups in high or low frequencies. However, these samples showed a small band at 3617  $\text{cm}^{-1}$  which is related to the vibration of the bridged hydroxyl groups, as a result of an incomplete ion exchange, in accordance with previous works [29,39].

Fig. 7 shows the infrared spectra for adsorbed carbon monoxide on the samples. For all cases, an intense vibration band at around 2084  $\text{cm}^{-1}$  is observed, corresponding to carbon monoxide species linearly adsorbed on Pt<sup>0</sup> species located within the zeolite

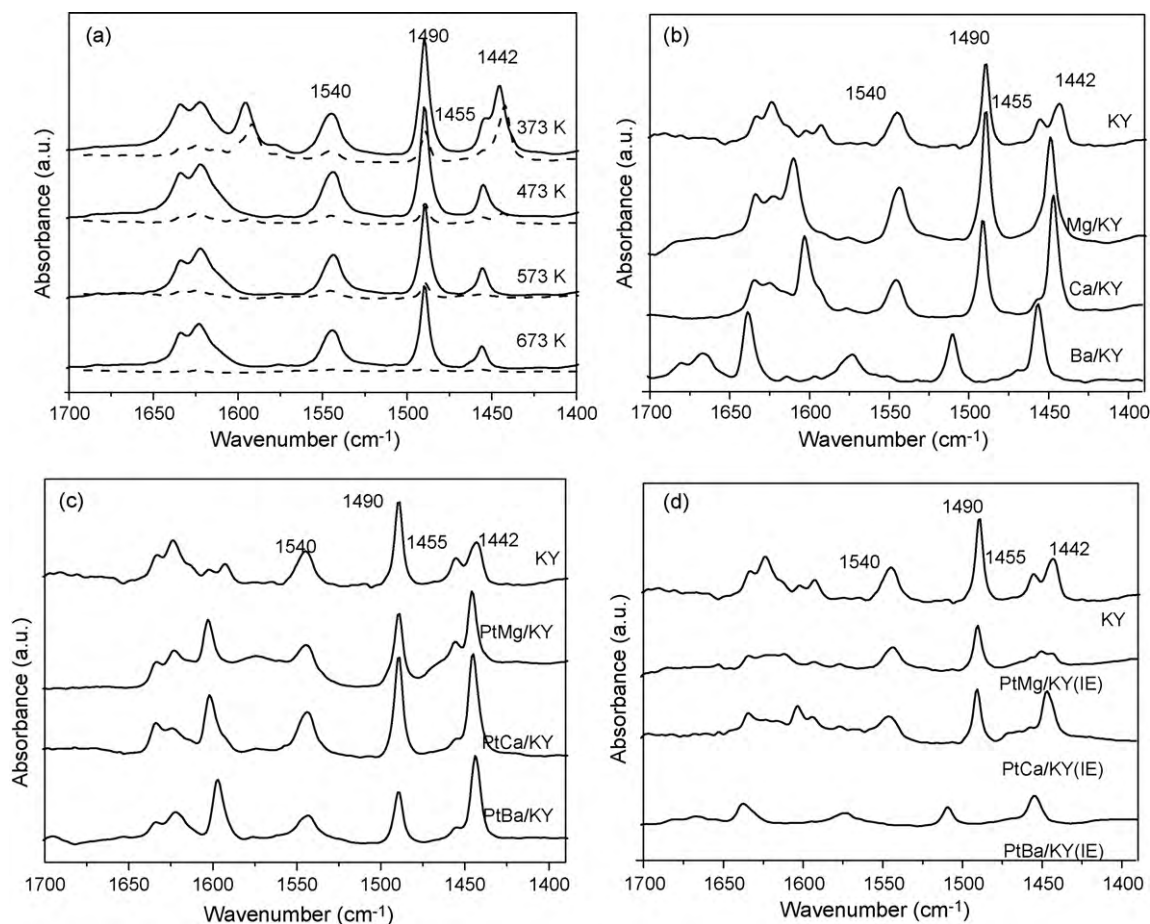


**Fig. 8.** (a) FTIR spectra recorded after pyridine adsorption/desorption at 373, 473, 573 and 673 K for the samples: (—) HY and (---) KY. FTIR spectra recorded after pyridine adsorption/desorption at 473 K (b) for the supports and for the catalysts (c) before and (d) after a second ion exchange.

channels most probably in the big cavity of the faujasite [40,41]. The catalysts containing magnesium and calcium showed a maximum for bands at  $2084\text{ cm}^{-1}$ , which is close to the value found for the KY zeolite-supported platinum. Nevertheless, for the barium-containing catalyst, an electronic interference occurs in the BaO–Pt interface, due to the highly basic character of barium oxide; this can explain the electron enrichment of platinum evidenced in the spectra by the decrease in the frequency related to the Pt–C≡O bond vibration [42,43]. Also, for this sample, as well as for that containing calcium, a shoulder can be observed at lower frequencies, indicating the presence of carbon monoxide adsorbed on electron-enriched platinum atoms in contact with negatively charged framework oxygen atoms [40,42]. For the Pt/KY and PtMg/KY samples, the band was narrower than the other ones, showing that they have more platinum species in the same electronic states, as compared to the catalysts containing calcium and barium, which showed wider bands.

The infrared spectra shown in Fig. 8(a) are related to HY and KY samples, after pyridine adsorption and its subsequent desorption at different temperatures. It is observed that the HY sample has Brønsted acid sites, whose characteristic band occurs near to  $1540\text{ cm}^{-1}$  and is related to pyridinium ions [36,44,45]. For this sample, Lewis acid sites are also present and are responsible for the absorption bands at  $1455$  and  $1442\text{ cm}^{-1}$  [36,44,45]. It is also noted that pyridine remained adsorbed on the Brønsted acid sites even after evacuation at 673 K, in accordance with previous work [46]. After desorption at 373 K, two bands are observed, which are related to pyridine adsorbed on Lewis acid sites. The band at lower frequency ( $1442\text{ cm}^{-1}$ ) disappeared after evacuation at 473 K, indi-

cating a weak interaction of pyridine with these sites. The intensity of the band at higher frequency ( $1455\text{ cm}^{-1}$ ) decreased upon heating, but did not disappear. Therefore, for the HY sample Brønsted acid sites are very strong, while Lewis acid sites show different strengths, which is probably related to the location of these sites in zeolite structure. For Y zeolite, with high Si/Al ratio, Jacobs and Beyer [47] ascribed the Lewis acid sites to extra-framework aluminum species, such as  $(\text{AlO}^+)$ . According to Yasuda et al. [48], a small amount of  $\text{SiO}_2\text{--Al}_2\text{O}_3$  in the amorphous phase, formed by a partial destruction of the zeolite structure, may contribute to the formation of Brønsted acid sites. For the KY sample, it can be observed that pyridine was completely desorbed from the Brønsted acid sites after evacuation at 673 K, showing that they are weaker than those observed for HY sample. Pyridine adsorbed on Lewis

**Table 2**  
Brønsted and Lewis acidity of the samples.

Sample	Brønsted sites ( $\mu\text{mol g}^{-1}$ )	Lewis sites ( $\mu\text{mol g}^{-1}$ )
HY	23.8	9.1
KY	4.0	4.4
Mg/KY	11.1	12.1
Ca/KY	5.9	13.0
Ba/KY	3.9	5.7
PtMg/KY	5.9	4.7
PtCa/KY	4.9	6.2
PtBa/KY	2.9	5.8
PtMg/KY(IE)	2.9	1.8
PtCa/KY(IE)	3.2	3.0
PtBa/KY(IE)	1.0	2.0

**Table 3**  
Metal dispersion (*D*) of fresh catalysts, drop in *n*-octane conversion ( $\Delta X$ ), coke deposited on the catalysts (*C*) and specific surface area of fresh (*S<sub>g</sub>*) and spent catalysts (*S<sub>g</sub><sup>\*</sup>*).

Sample	<i>D</i> (%)	$\Delta X$ (%)	<i>C</i> (%)	<i>S<sub>g</sub></i> (m <sup>2</sup> g <sup>-1</sup> )	<i>S<sub>g</sub><sup>*</sup></i> (m <sup>2</sup> g <sup>-1</sup> )
Pt/KY	–	30	0.105	708	325
PtMg/KY	59	30	0.075	629	348
PtCa/KY	47	42	0.060	610	389
PtBa/KY	59	23	0.064	482	344

acid sites (1455 and 1442 cm<sup>-1</sup>) was almost completely desorbed at 473 K and the peaks disappeared at higher temperatures. This sample still had Brønsted and Lewis acid sites after going through ion exchange, but they were much weaker than the ones of the HY sample.

The spectra for the supports and for the catalysts containing promoters after pyridine desorption at 473 K are the same as for KY sample (Fig. 8). It can be seen that the supports and catalysts have both Lewis and Brønsted acid sites and there is an increment in peak intensity, at 1442 cm<sup>-1</sup> (weak Lewis sites) when compared to KY sample.

It can also be seen that the concentration of Lewis and Brønsted acid sites increased with the introduction of magnesium in the KY sample. Similar results were observed with calcium but the addition of barium only increased the intensity of the band related to Lewis acid sites. The intensity increase for the band at 1442 cm<sup>-1</sup> is related to pyridine adsorption on the Mg<sup>2+</sup>, Ca<sup>2+</sup> and Ba<sup>2+</sup> cations [49]. Besides, during impregnation, some K<sup>+</sup> species could be exchanged by these cations or some MOH<sup>+</sup> species could be produced, which can also work as Lewis acid sites [36,49].

The concentrations of the Lewis acid sites and Brønsted acid sites (Table 2) were measured in terms of the amount of pyridine adsorbed on the catalysts at 473 K; the areas of vibration bands related to Brønsted and Lewis acid sites were calculated from 1560 to 1530 cm<sup>-1</sup> and from 1465 to 1430 cm<sup>-1</sup>, respectively [50]. As expected, the Brønsted acid sites concentration for HY zeolite decreased after ion exchange. However, an increase in the amount of Lewis and Brønsted acid sites after impregnating the KY zeolite with magnesium and calcium was detected, a fact which can be related to the hydrolysis of Mg<sup>2+</sup> and Ca<sup>2+</sup> cations; this effect was stronger for the sample with magnesium, which has the highest ionic potential. By adding platinum, there was a reduction of Lewis and Brønsted acid sites, which suggests that platinum was adsorbed on such sites. Yet, for the Ba/KY sample such significant increase was not observed for the concentration of acid sites; after the addition of platinum and a further ion exchange, carried out after platinum impregnation, this concentration decreased as shown by the PtMg/KY(T) sample. For the other samples, PtMg/KY(T) and PtCa/KY(T), the Brønsted acid sites also remained in the solids, which means that the ion exchange was not completely efficient. Table 3 shows the metal dispersion values. The catalysts with magnesium and barium showed the same dispersion (59%) while the one containing calcium showed a lower value (47%). These results can be correlated with the properties of the promoter ions. The Ba<sup>2+</sup> ions are too large to go into the smaller cages (sodalite and hexagonal prisms) while the Mg<sup>2+</sup> ions undergo hydrolysis and are able to block the sodalite cages but not the hexagonal prisms; on the other hand, the Ca<sup>2+</sup> ions easily block both the sodalite cages and hexagonal prisms [51]. Therefore, in magnesium and barium-containing samples, platinum occupies the smaller cages (sodalite cages and hexagonal prisms), which leads to the highest dispersions. For the calcium-containing sample, that does not occur and platinum is concentrated in the zeolite supercages showing the lowest dispersion.

All catalysts were active in *n*-octane reforming at 723 K, as shown in Fig. 9. It is well known that when platinum is highly dispersed on the support, it is responsible for the aromatization

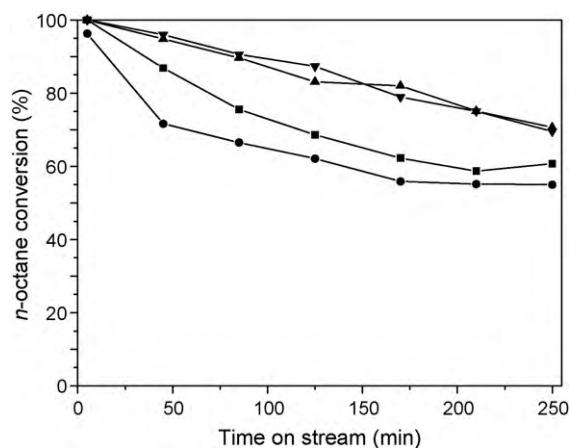


**Fig. 9.** Conversion of *n*-octane over the catalysts as a function of time reaction. (–▼–) Pt/KY, (–▲–) PtMg/KY, (–●–) PtCa/KY and (–■–) PtBa/KY.

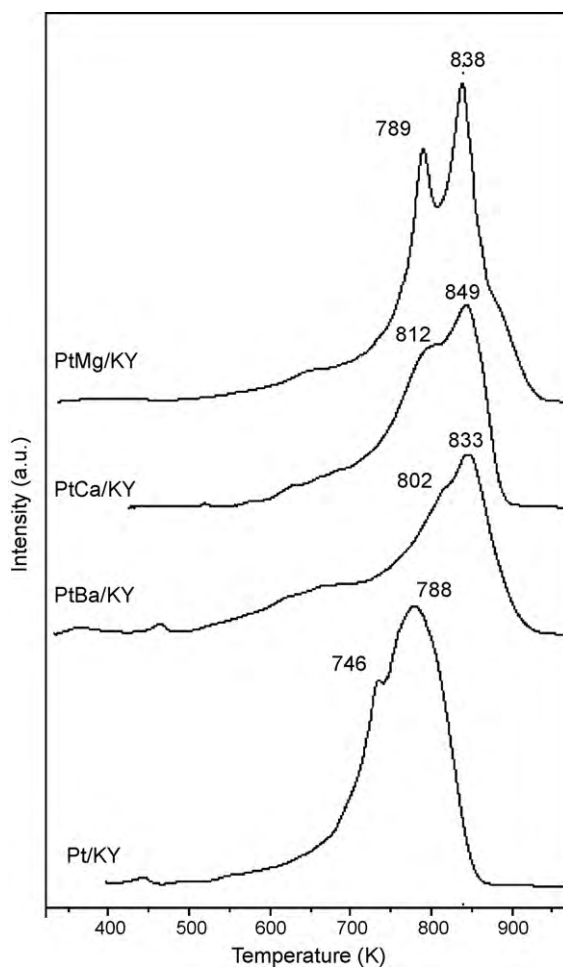


**Fig. 10.** TPO profiles for the catalysts.

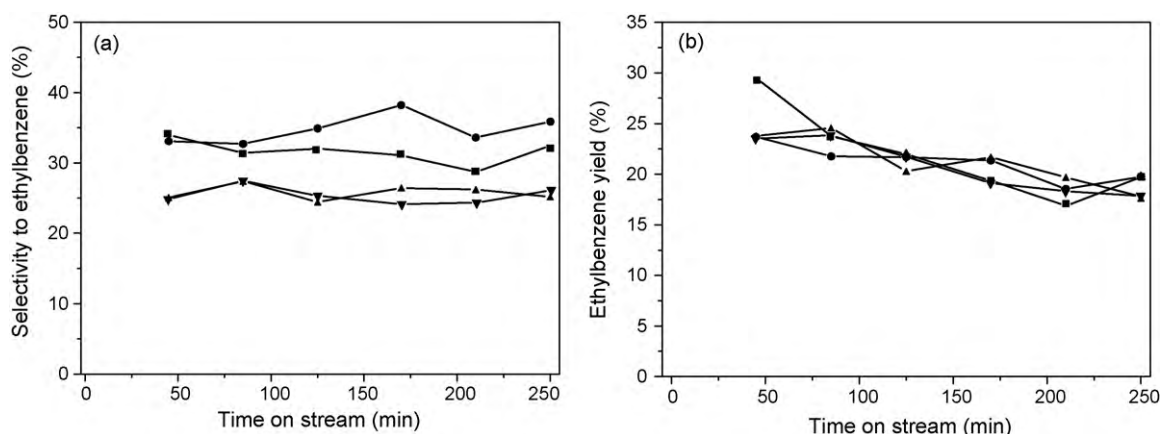


Fig. 11. (a) Selectivity to ethylbenzene and (b) ethylbenzene yield for the catalysts: (–▼–) Pt/KY, (–▲–) PtMg/KY, (–●–) PtCa/KY and (–■–) PtBa/KY.

of linear hydrocarbon chains, which are present in naphtha cuts [12], because of its ability of breaking relatively strong bonds, such as H–C and forming Pt, Pt–H and Pt–C bonds [52]. This can explain the highest initial conversion of magnesium and barium-containing catalysts, which have the highest dispersions.

However, during reaction the *n*-octane conversion continuously dropped and the samples with barium and calcium led to about 60% and 55%, after 175 min reaction, respectively. The solid without any dopant and that containing magnesium showed the highest conversion after 50 min on stream, achieving almost 70% conversion after 175 min time-on-stream. The drop in conversion can be related to coke deposition as well as to the decrease in specific surface area during reaction; however, no simple relationship was found among them, as shown in Table 3. As we can see, the highest amount of coke was deposited on magnesium-containing catalyst and on the dopant-free sample, which also showed the highest decrease in specific surface area. However, as shown in Fig. 10, some coke was deposited on outer surface of zeolite and seems not to affect the activity of the catalyst. As pointed out previously [53], the first peak in TPO can be assigned to coke deposited outside the channels while the high temperature peak is related to coke deposited inside the channels. On the other hand, the barium or calcium-containing catalysts have similar amounts of coke but the calcium-containing sample has the hardest coke (Fig. 10), which is inside the channels and is difficult to burn (849 K) [53]; this can explain why this sample led to the highest drop in conversion.

It has been largely accepted that, in the conditions of catalytic reforming of high alkanes, the aromatization of *n*-octane can occur according to both monofunctional (only metal) and bifunctional (acid–metal) mechanism [15,25]. From Table 4, which shows the

selectivity to the products of the *n*-octane reforming reaction after 250 min of reaction, we can see the predominant formation of ethylbenzene and *o*-xylene, indicating that the monofunctional mechanism occurred on the catalysts. By this pathway, octane goes on dehydrogenation to produce octene followed by 1–6 or 2–7 ring closure and then the dehydrogenation of cyclized compounds to produce ethylbenzene and *o*-xylene; alternatively, octane is dehydrogenated into mono, di and triene, followed by terminal ring [25,54]. However, isomers (*i*-C<sub>4</sub>–*i*C<sub>8</sub>, *m*-xylene) as well as cracking and hydrogenolysis products (C<sub>1</sub>, C<sub>2</sub>–C<sub>7</sub>) were also detected, indicating the occurrence of the bifunctional mechanism on the catalysts, as a consequence of their residual acidity. According to this mechanism, *n*-octane is first dehydrogenated on the metal and then the terminal ring closure occurs on acidic site of the support. Side reactions, such as cracking and isomerization, also take place on the acid sites of the support, which are usually faster than dehydrogenation, leading to a large number of products [25].

The barium-containing catalyst was expected to be the most selective to aromatics, since it is believed that the basicity of the catalyst increases the electron density of platinum and thus promotes the aromatization of *n*-octane [42]. In fact, the experiments of chemisorbed carbon monoxide confirmed that this sample contains the electron-enriched platinum species, as compared to the others. However, calcium was the most efficient promoter for improving aromatization and this can be related to the role of acidic sites in favoring the bifunctional mechanism, the ring closure occurring on the acidic sites.

From Table 4, it can also be seen that the ethylbenzene to *o*-xylene ratio is closed to one for the Pt/KY and PtMg/KY catalysts, meaning that there is not mass transfer limitation inside the channels on the zeolite [14]. This ratio increased to 1.4 and 1.5, for PtCa/KY to PtBa/KY, respectively, indicating that there is pore restriction in this order, in accordance with the textural properties of the catalysts. As pointed out early [14,16], since *o*-xylene has a larger kinetic diameter than ethylbenzene, it has more difficulty in leaving the pore, after it has been produced. As a result, *o*-xylene would preferentially convert to benzene and toluene before going out from the pore. Based on these arguments, it would be expected that the PtMg/KY would produce less benzene and toluene but these products also comes from the bifunctional mechanism that also occurs in some extension.

Fig. 11 shows the selectivity to ethylbenzene displayed by the catalysts, as a function of reaction time. The catalysts containing calcium and barium were the most selective, after 50 min of reaction, a fact which can be related to the presence of electron-enriched platinum due to promoters, as found by CO-FTIR spectra, in accordance with previous work [42]. However, from the curve of

Table 4  
Dehydrocyclization of *n*-octane over the catalysts after 250 min on stream.

Selectivity <sup>a</sup>	Pt/KY	PtMg/KY	PtCa/KY	PtBa/KY
C <sub>1</sub>	0.1	0.3	0.1	0.5
C <sub>2</sub> –C <sub>7</sub>	1.4	1.7	0.5	3.0
<i>i</i> C <sub>4</sub> – <i>i</i> C <sub>9</sub>	13	16	15	17
CC <sub>5–8</sub>	0.7	0.8	0.6	1.7
Bz	0.5	1.3	0.1	1.8
Tol	2.8	6.7	2.0	7.3
EB	26	25	36	32
<i>p</i> -X	7.4	3.8	2.6	3.5
<i>m</i> -X	26	20	17	12
<i>o</i> -X	23	24	26	21
AroT	85	81	84	78

<sup>a</sup> C<sub>1</sub>: methane; C<sub>2</sub>–C<sub>7</sub>: linear alkanes C<sub>2</sub>–C<sub>7</sub>; *i*C<sub>4</sub>–*i*C<sub>9</sub>: isomers C<sub>4</sub>–C<sub>9</sub>; CC<sub>5–8</sub>: cycloalkanes C<sub>5</sub>–C<sub>8</sub>; Bz: benzene; Tol: toluene; EB: ethylbenzene; *p*-X: *p*-xylene; *m*-X: *m*-xylene; *o*-X: *o*-xylene and AroT: total aromatics.

ethylbenzene yield, it can be noted that the low ethylbenzene selectivity for the magnesium-containing catalyst was compensated by its high conversion, resulting in yields close to those of the other catalysts, along all the reaction time.

#### 4. Conclusions

Catalysts based on platinum supported on KY zeolite modified with calcium, barium and magnesium, are suitable to produce ethylbenzene by *n*-octane conversion. The magnesium-containing catalyst showed the highest *n*-octane conversion while the calcium-containing catalyst showed the highest selectivity to ethylbenzene but the hardest coke, which led to the highest drop in conversion. As a whole, the catalysts showed similar yields of ethylbenzene. The *n*-octane conversion is supposed to occur by both monofunctional and bifunctional mechanism due to the residual acidity of the catalysts.

#### Acknowledgments

JSLF thanks CAPES for her scholarship. The authors thank Professor Rosane Gil (DQO-IQ-UF RJ), for the RMN analyses and to the CNPq and FINEP for the financial support.

#### References

- [1] T.F. Degnan Jr., C.M. Smith, C.R. Venkat, Appl. Catal. A: Gen. 221 (2001) 283–294.
- [2] Y. Du, H. Wang, S. Chen, J. Mol. Catal. A: Chem. 179 (2002) 253–261.
- [3] M.S. Ramos, M.S. Santos, L.P. Gomes, A. Albornoz, M.C. Rangel, Appl. Catal. A: Gen. 341 (2008) 12–17.
- [4] A.C. Oliveira, J.L.G. Fierro, A. Valentini, P.S.S. Nobre, M.C. Rangel, Catal. Today 85 (2003) 49–57.
- [5] S.-G. Yoon, J. Lee, S. Park, Appl. Therm. Eng. 27 (2007) 886–893.
- [6] C. Perego, P. Ingallina, Catal. Today 73 (2002) 3–22.
- [7] G. Bellussi, G. Pazzuconi, C. Perego, G. Girotti, G. Terzoni, J. Catal. 157 (1995) 227–234.
- [8] M.C. Rangel, C.L. Pieck, G. Pecchi, N.S. Figoli, P. Reyes, Ind. Eng. Chem. Res. 40 (2001) 5557–5563.
- [9] J.M. Parera, N.S. Figoli, in: G.J. Antos, A.M. Aitani, J.M. Parera (Eds.), Catalytic Naphtha Reforming: Science and Technology, Marcel Dekker Inc., New York, 1995, p. C. 3.
- [10] M.C.S. Santos, J.M. Grau, C.L. Pieck, J.M. Parera, J.L.G. Fierro, N.S. Figoli, M.C. Rangel, Catal. Lett. 103 (2005) 229–237.
- [11] M.C. Rangel, L.S. Carvalho, P. Reyes, J.M. Parera, N.S. Figoli, Catal. Lett. 64 (2000) 171–178.
- [12] I.Z. Paál, G.J. Antos, in: A.M. Aitani, J.M. Parera (Eds.), Catalytic Naphtha Reforming: Science and Technology, Marcel Dekker Inc., New York, 1995, p. C. 2.
- [13] C.L. Pieck, C.R. Vera, J.M. Parera, G.N. Gimenez, L.R. Serra, L.S. Carvalho, M.C. Rangel, Catal. Today 107 (2005) 637–642.
- [14] S. Jongpatiwut, S. Trakarnroek, T. Rirksomboon, S. Osuwan, D.E. Resasco, Catal. Lett. 100 (2005) 7–15.
- [15] S. Jongpatiwut, P. Sackamduang, T. Rirksomboon, S. Osuwan, D.E. Resasco, J. Catal. 218 (2003) 1–11.
- [16] S. Trakarnroek, S. Jongpatiwut, T. Rirksomboon, S. Osuwan, D.E. Resasco, Appl. Catal. A: Gen. 313 (2006) 189–199.
- [17] E. Iglesia, S.L. Soled, G.M. Kramer, J. Catal. 144 (1993) 238–253.
- [18] G. Jacobs, C.L. Padro, D.E. Resasco, J. Catal. 179 (1998) 43–55.
- [19] D.L. Hoang, H. Preiss, B. Parltitz, F. Krumeich, H. Lieske, Appl. Catal. A 182 (1999) 385–397.
- [20] A. Trunschke, D.L. Hoang, J. Radnik, K.-W. Brzezinka, A. Brückner, H. Lieske, Appl. Catal. A: Gen. 208 (2001) 381–392.
- [21] B.H. Davis, J. Catal. 42 (1976) 376–380.
- [22] D.L. Hoang, S.A.-F. Farrage, J.M.-M. Radnikpohl, M. Schneider, H. Lieske, A. Martin, Appl. Catal. A: Gen. 333 (2007) 67–77.
- [23] P. Mériaudeau, A. Thangaraj, C. Naccache, S. Narayanan, J. Catal. 146 (1994) 579–582.
- [24] H. Armendariz, A. Guzman, J.A. Toledo, M.E. Llanos, A. Vásquez, G. Aguillar-Rios, Appl. Catal. A: Gen. 211 (2001) 69–80.
- [25] A. Szechenyi, F. Solymosi, Appl. Catal. A: Gen. 306 (2006) 149–158.
- [26] M. Guisnet, F.R. Ribeiro, Zeólitos: um nanomundo ao serviço da catálise, Fund. Calouste Gulbenkian, Lisboa, 2004.
- [27] M.S. Ramos, S.T.F. Grecco, L.P. Gomes, A.C. Oliveira, P. Reyes, M. Oportus, M.C. Rangel, Stud. Surf. Sci. Catal. 156 (2005) 809–814.
- [28] J.R. Sohn, S.J. DeCanio, J.H. Lunsford, D.J. O'Donnell, Zeolites 6 (1986) 225–227.
- [29] L. Pinard, J. Mijoin, P. Magnoux, M. Guisnet, J. Catal. 215 (2003) 234–244.
- [30] D.H. Everett, IUPAC Definitions, Terminology and Symbols in Colloid and Surface Chemistry, Part I, Pure Appl. Chem. 31 (1972) 579–638.
- [31] P. Horcajada, C.M. Alvarez, A. Rámila, J.P. Pariente, M.V. Regí, Solid State Sci. 8 (2006) 1459–1465.
- [32] E. Lippmaa, M. Magi, A. Samoson, M. Tarmak, G. Engelhardt, J. Am. Chem. Soc. 103 (1981) 4992–4996.
- [33] J. Datka, B. Gil, T. Domagala, K.G. Marek, Microporous Mesoporous Mater. 47 (2001) 61–66.
- [34] E.M. Flanigen, H. Khatami, H.A. Szymanski, Molecular Sieve Zeolites, in: Adv. Chem. Ser., vol. 101, American Chemical Society, Washington, DC, 1971.
- [35] E.F.S. Aguiar, V.L.D. Camorim, F.M.Z. Zotin, R.L.C.A. Santos, Microporous Mesoporous Mater. 25 (1998) 25–34.
- [36] D.W. Breck, Zeolite Molecular Sieves: Structure, Chemistry and Use, Robert E. Krieger Publishing Company, Malabar, 1984.
- [37] D. Barthomeuf, Catal. Rev. Sci. Eng. 38 (1996) 521–612.
- [38] F. Thibaut-Starzyk, B. Gil, S. Aiello, T. Chevreau, J.-P. Gilson, Microporous Mesoporous Mater. 67 (2004) 107–112.
- [39] M. Bevilacqua, T. Montanari, E. Finocchio, G. Busca, Catal. Today 116 (2006) 132–142.
- [40] G.S. Lane, J.T. Miller, F.S. Modica, M.K. Barr, J. Catal. 141 (1993) 465–477.
- [41] P. Kubanek, H.-W. Schmidt, B. Spliethoff, F. Schüth, Microporous Mesoporous Mater. 77 (2005) 89–96.
- [42] J.M. Grau, X.L. Seoane, A. Arcoya, Catal. Lett. 83 (2002) 247–255.
- [43] E.A. Cotton, G. Wilkinson, Advances in Inorganic Chemistry, Wiley-Interscience, New York, 1967.
- [44] G. Coudurier, F. Lefebvre, in: B. Imelik, J.C. Vedrine (Eds.), Catalyst Characterization: Physical Techniques for Solid Materials, Plenum Press, New York, 1994.
- [45] R. Anuradha, M. Palanichamy, V. Murugesan, J. Mol. Catal. A: Chem. 272 (2007) 198–206.
- [46] M.L. Occelli, P. Ritz, Appl. Catal. A: Gen. 183 (1999) 53–59.
- [47] P.A. Jacobs, H.K. Beyer, J. Phys. Chem. 83 (1979) 1174–1177.
- [48] H. Yasuda, T. Sato, Y. Yoshimura, Catal. Today 50 (1999) 63–71.
- [49] J.W. Ward In: J.A. Rabo, Zeolite Chemistry and Catalysis, American Chemical Society, Washington, 1976, C. 3.
- [50] C.A. Emeis, J. Catal. 141 (1993) 347–354.
- [51] W.M.H. Sachtler, Z. Zhang, Adv. Catal. 39 (1993) 129–213.
- [52] G.A. Somorjai, Introduction to Surface Chemistry and Catalysis, John Wiley & Sons, Inc., New York, 1994.
- [53] S.M. Domingues, J.M. Britto, A.S. de Oliveira, A. Valentini, P. Reyes, J.M. David, M.C. Rangel, Stud. Surf. Sci. Catal. 139 (2001) 45–52.
- [54] P. Mériaudeau, C. Naccache, Catal. Rev. Sci. Eng. 39 (1997) 5–48.